Nozzle-Lip Effects on Argon Expansions Into the Plume Backflow

David H. Campbell*
University of Dayton Research Institute, Astronautics Laboratory (AFSC), Edwards Air Force Base, California

The structure of the flow of argon through a 2-cm-long, 4-mm-diam tube, around the tube lip, and into vacuum has been investigated using the Direct Simulation Monte Carlo technique. Two lip geometries have been compared, and the shape and thickness of the lip were found to have a significant influence on the flowfield structure and the total flux into the backflow. The effects of the temperature and scattering characteristics of the front lip surface were investigated and found to affect the backflow only for certain lip shapes. The number density and temperature of the gas were also found to have a significant effect on the backflow due to changes in the collisional processes in the expansion flow, which affects the freezing of the parallel component of the random motion of the gas.

Introduction

THE expansion of gases out of a rocket nozzle or outgassing orifice into a low-density background is an important problem with importance to spacecraft contamination, heat transfer, and infrared sensor interference. The expansion of gases around the nozzle lip and into the region upstream of the nozzle exit plane, usually referred to as the backflow region, is a particularly complex gas dynamic problem. It has been recognized for many years[1-6] that the expansion of the subsonic and lower Mach number supersonic regions of the boundary layer around a nozzle lip can produce significant flux into the high-angle backflow region not predicted by the conventional Prandtl-Meyer uniform supersonic flow analysis. It has recently been recognized that nonequilibrium effects,[7] due to the rapid rarefaction of the flow out of a nozzle exiting to vacuum or near vacuum, can affect the structure of the flow around a nozzle lip. Consequently, accurate modeling of the flowfield around a nozzle lip and into the high-angle backflow region cannot be obtained using standard equilibrium gas dynamic models. The Direct Simulation Monte Carlo (DSMC) modeling technique,[8] which models a gas flow by following some representative number of molecules through simulated collisions, does account for nonequilibrium effects, and is essentially the only technique presently available for accurate prediction of these flows.

The shape of the nozzle lip may play an important role in determining the flux into the backflow. Pipes et al.[9] observed some effects of nozzle-lip shape on the flowfield at the exit plane for carbon dioxide and nitrogen expansions from small nozzles, with a pronounced dependence of the effect on the level of condensation in the flow. Direct evidence of lip shape effects on flow into the backflow region was observed by Chirivella[10] for pure nitrogen flows. Hueser et al.[11] used the DSMC technique to study the detailed flowfield around the nozzle lip for conditions simulating the inertial upper stage IUS motor at 282-km altitude. They found large differences between the flowfield predicted by the DSMC technique and that predicted by the equilibrium Method of Characteristics technique. They modeled a nozzle lip with finite thickness, but investigated only one lip shape and one lip thickness for one set of initial flow conditions.

The results of a detailed DSMC theoretical analysis of the effects of lip shape and lip thickness on the flowfield around the lip of a nozzle with zero half angle (tube) will be presented in this paper. In addition, the effects of upstream conditions (gas density and temperature), front lip surface temperature, and front lip surface accommodation coefficient on the backflow structure have been investigated and will be described. As will be shown, the degree of translation nonequilibrium in the gas expansion, which is dependent on the gas density and temperature, can significantly affect the structure and degree of backflow. In addition, translation nonequilibrium processes interact with the different lip shapes and thicknesses in a nonsimple manner.

Model Description

To investigate the effects of nozzle lip shape and thickness, the DSMC technique was used to map the flow of argon into vacuum through a 2-cm-long tube of 2-mm radius for two lip shapes (Fig. 1) and for wall thicknesses from 0 to 2.0 mm. Because of the extremely large change in gas number density from the internal flow to the far backflow region, the calculations are conducted in four steps. The first uses a finite-difference Navier-Stokes code (VNAP2)[12] to calculate the internal flow to a position 2 mm upstream of the tube exit plane. The DSMC code is then used to calculate the flow from that position to a position 0.15 mm upstream of the tube exit plane. The influence of the tube lip thickness on the flow at this start line was checked and found to be negligible for all of the flow parameters. The third step is a full DSMC calculation from the start line 0.15 mm inside the tube out into the forward flow and around the lip into the backflow region. The run is allowed to proceed until good statistics are obtained in

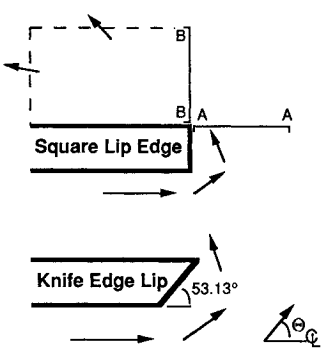

Fig. 1 Lip shapes. Flow angle convention is also shown. A-A and B-B are longitudinal and radial profiles presented in figures to follow. Dotted lines indicate boundary cells used for backflow flux calculation.

Received Nov. 17, 1988; revision received Feb. 13, 1989.

*Research Physicist. Member AIAA.

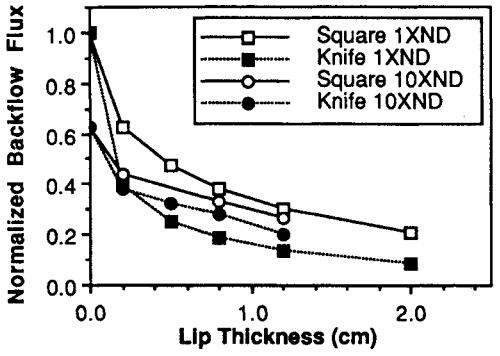

Fig. 2 Normalized flux into backflow region. Dependence on lip shape, lip thickness, and starting gas number density. Flux is normalized by number density multiplier.

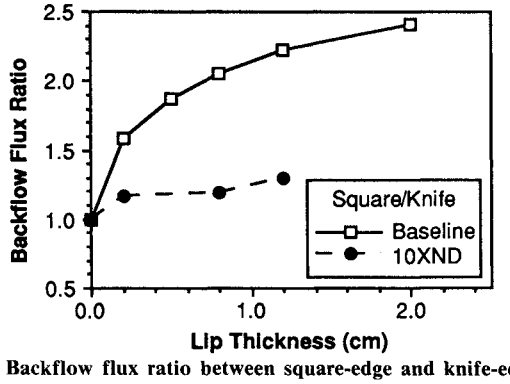

Fig. 3 Backflow flux ratio between square-edge and knife-edge lip shapes.

the region directly in front of the lip, but not long enough to produce good statistics in the backflow region. The final step is a calculation of the flow from a horizontal line along the inner edge of the lip out into the backflow region, using the results of step 3 for the input start conditions at that line. Again, the influence of the lip thickness on the startline conditions was checked and found to be negligible for all of the flow parameters, i.e., the nozzle lip had no influence on the conditions upstream of the inner edge of the lip. Consequently, the same start-line was used for all lip thicknesses. For one case the third step was allowed to run long enough to obtain good statistics in the backflow region in order to check the effect of using a restart along the horizontal line at the inner edge of the lip. Since the restart file only supplies the average flow quantities of velocity and temperature, if any significant nonequilibrium in the translational mode exists at this position, it would not be tracked upon restarting the code. No significant difference was found between the restart results and the full-field results.

The cell structure used in the calculations was the final configuration reached after a number of iterations. The mean free path must be at least 2–3 times greater than the cell size to avoid flow smearing, and the mean collision time must be 2–3 times greater than the time step for the calculation to track changes in the flow parameters accurately. The cells were adjusted so that the flowfield and cell structure met or exceeded these criteria in all cells except for those cells far from the lip in the forward flow region, where the mean free path was slightly less than the cell diameter. The flowfield is slowly varying in those regions, so that no flow smearing was expected due to the low ratios.

The effects of random number seed value, cell number, and size (within the preceding limits), and number of simulated atoms were investigated and found to be small in all cases. With respect to the effects of the number of simulated atoms, that number was kept approximately the same for all runs (about 7000 for the last DSMC step as previously described), which resulted in about 10 particles per cell.

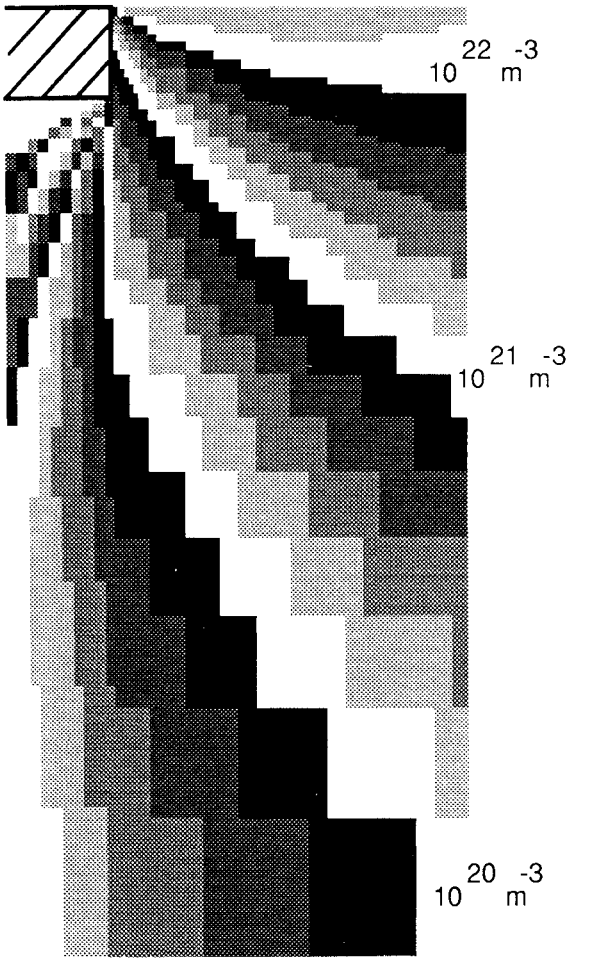

Fig. 4 Number density distribution for square lip. Log scaling is used.

A stagnation temperature of 300 K and a stagnation pressure of 1 KPa (7.5 Torr) were the standard conditions used in the calculations. Diffuse reflection (full accommodation) of gas particles from the tube walls was used for all gas/wall interactions except for one series of runs where specular reflection was used for the front lip surface to investigate the effects of the surface interaction model. A thick boundary layer develops for these conditions (Reynolds number ~500 at the tube end) and fills a large portion of the tube at the exit plane.

Effects of Lip Shape and Thickness

One measure of the effect of lip shape and thickness is the total amount of flux into the backflow region. In this paper the total backflow flux will be defined as the flux (number density × velocity × subtended angle) calculated for each outer boundary cell summed for those cells with flow angles of 90 deg or greater (Fig. 1). In Fig. 2 the relative flux of argon into the backflow region is shown. Both tube lip thickness and shape have pronounced effects on the backflow flux. From these results it can be concluded that the scattering from the front face of the lip has a significant effect on the flux of gas into the backflow region for these flow conditions. Thicker lips produce more forward scattering, i.e., flow angles directed more toward the forward flow direction, which reduces the number of atoms scattered into the backflow. The knife-edge lip shape scatters more atoms into the forward flow direction than the square edge lip, and thus produces less backflow flux. The ratio of the backflow flux between the square and knife edge lips is shown in Fig. 3. The ratio increases with increasing lip thickness and appears to be leveling off at a value of approximately 2.5 for this baseline condition.

The complete flowfield number density distribution is shown in gray scale format in Fig. 4 for the 0.8-mm-square

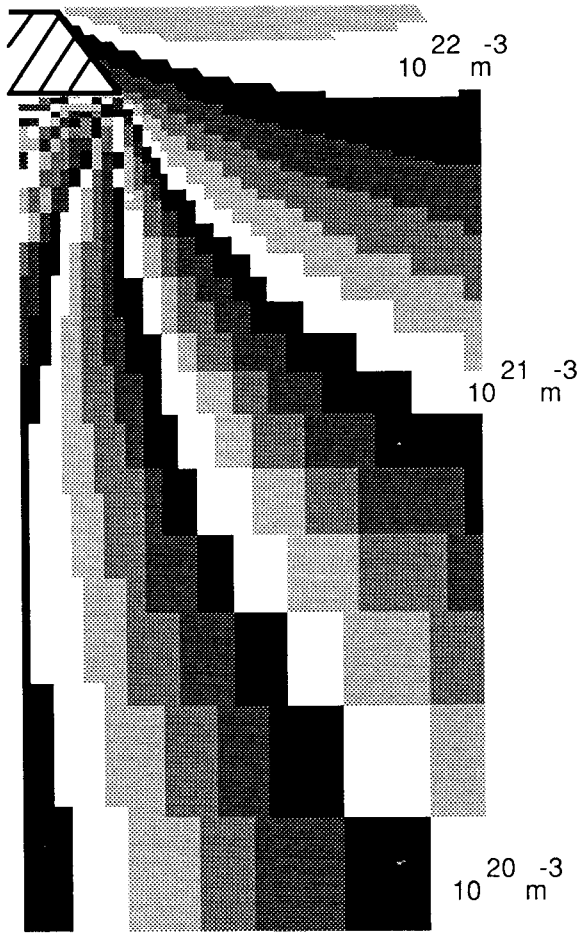

Fig. 5 Number density distribution for knife-edge lip. Log scaling is used.

lip, and in Fig. 5 for the 0.8-mm knife-edge lip. Only the flow in front of the lip and into the backflow is presented, since the forward flow region is identical for the two cases. Rarefaction is very fast near the outer edge of the lip for both cases. The flow for the knife-edge lip expands more slowly in front of the lip, but faster around the outer lip edge than the square lip. This is illustrated more clearly in Figs. 6 and 7. In Fig. 6, a horizontal profile of the number density along a line at the position of the outer edge of the lip is shown (profile A-A in Fig. 1). The number density for the knife-edge lip is much greater (and, therefore, the gas has expanded more slowly) than that for the square lip out to a distance of about 4 mm from the wall, at which point the lip shape no longer influences the flowfield.

Despite the much larger number density in front of the lip for the knife edge, the total flux into the backflow region is much lower for the knife edge than for the square lip (Fig. 2). The reason for this is illustrated in Fig. 7, where the flow angle is shown along the horizontal line at the outer edge of the lip (profile A-A). The flow angle is much lower for the knife-edge lip, which results in more of the flow being directed in the forward direction (< 90 deg) for the knife-edge lip than for the square lip.

A more detailed look at the flowfield into the backflow region is shown in Fig. 8 for the square lip. The unit flux (gas particles per square meter per second) of argon gas into the backflow along profile B-B peaks at a position within 1 mm of the wall, with the peak position moving farther out as lip thickness increases. The value of the unit flux drops significantly near the wall as the lip thickness increases. At large distances from the wall the unit flux converges to a constant value. A similar behavior was found for the knife-edge lip.

One might, therefore, conclude that by employing a knife-edge lip, it is possible to reduce the backflow flux by a factor

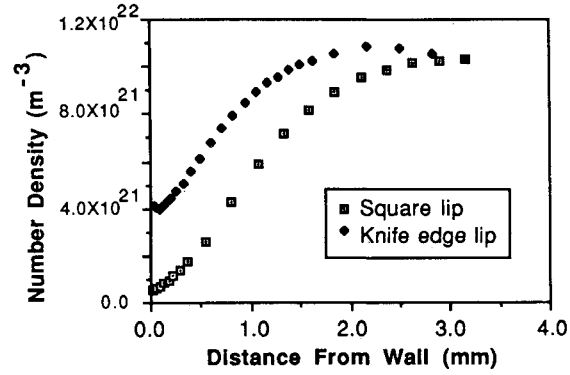

Fig. 6 Number density profile along A-A for 0.8-mm-thick lip.

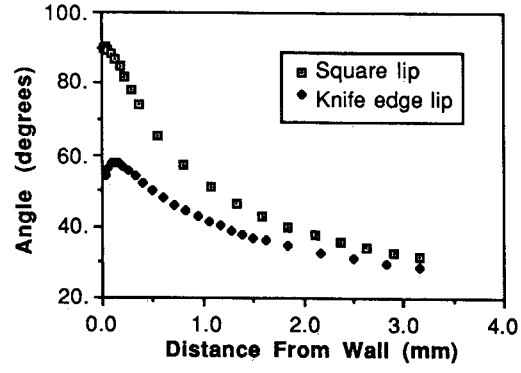

Fig. 7 Angle profile along A-A for 0.8-mm lip.

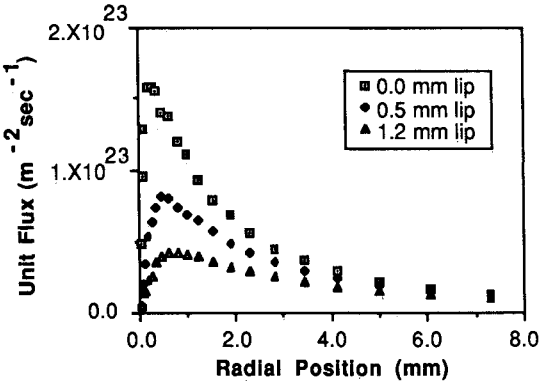

Fig. 8 Unit flux along B-B for square lip.

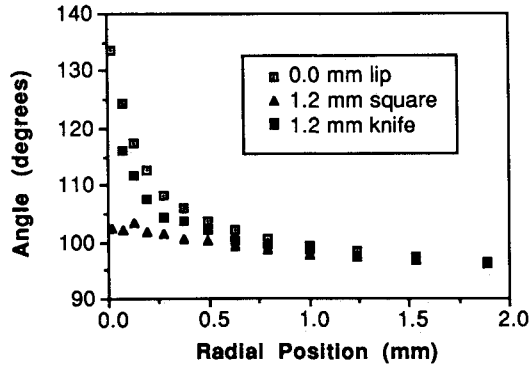

Fig. 9 Flow angle along B-B.

of about 2 and, consequently, reduce potential spacecraft contamination by a similar factor. Unfortunately, the total flux is only one parameter contributing to the potential for contamination or other unwanted effects. In Figs. 9 and 10 we illustrate the difference between the flow angle along profile B-B in the backflow region for the square and knife-edge lips.

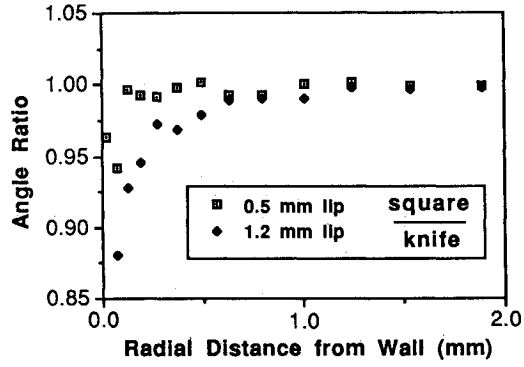

Fig. 10 Angle ratio comparison for knife-edge and square lips and two lip thicknesses along B-B.

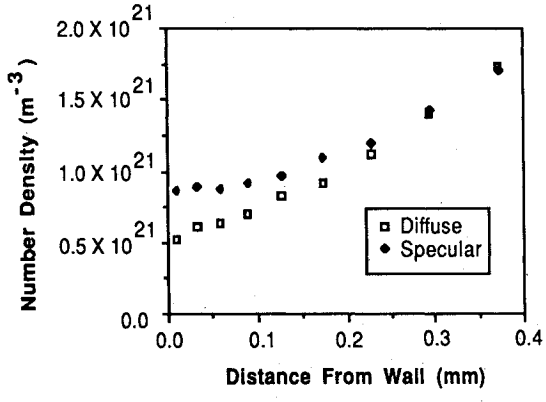

Fig. 11 Number density profile along A-A for 0.8-mm-square lip.

Table 1 Relative backflow flux for different surface reflection types (0.8-mm lip)

	Diffuse	Specular
Square	1.0	1.005
Knife	0.485	0.175

For the thicker lips, the angle near the wall is larger for the knife-edge lip than it is for the square lip, despite the fact that the flow angle in front of the lip starts out at a much lower value for the knife-edge lip (Fig. 7). For the knife-edge case, the expansion is more like the zero-thickness lip (Fig. 9), which produces higher-angled flow in the backflow region than thicker lips. Depending on the particular phenomenon of concern, this increased angle may counter any benefit gained from the decreased flux of knife-edge lips compared to square lips.

Effects of Lip Surface Characteristics

Since it is clear from the preceding results that gas scattering off the front of the lip has a pronounced effect on the backflow, the characteristics of the collisional interaction of gas particles with the front of the lip have been investigated. The effects of the type of wall interaction and of wall surface temperature on the backflow structure are presented in this section.

Type of Wall Reflection

To investigate the effects of the type of wall interaction, calculations were made for 0.8-mm-thick square and knife-edge lips using full specular reflection from the front face of the lip. In these calculations, there is no energy exchange between the gas particles and surface during a collision with the wall. The colliding particles simply reflect off the wall with only a change in their direction of motion. This is in contrast to all of the previous results, which used diffuse reflection

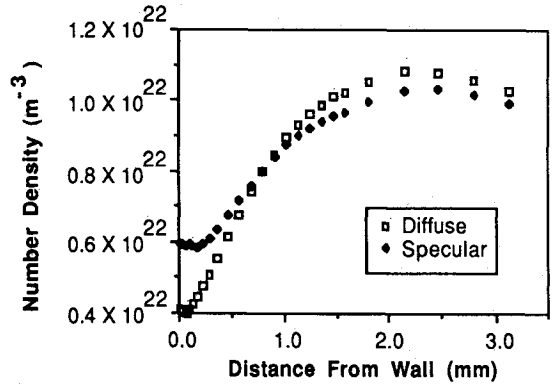

Fig. 12 Number density profile along A-A for 0.8-mm-knife-edge lip.

from all walls. With diffuse reflection, particles that collide with the walls are assumed to fully accommodate with the wall conditions and leave the wall with a statistical distribution of energy corresponding to the wall temperature, which is a constant 300 K in all of the calculations. The relative backflow flux for diffuse and specular reflection from the front face of the lip for both the square and knife-edge lip is compared in Table 1. From these results it is clear that the type of interaction with the front face of the lip does not affect the backflow for the square-edge lip, but has a pronounced influence on the backflow for the knife-edge lip.

The angle profile in the backflow region at the exit plane (profile B-B) for the square-edge lip was identical for specular and diffuse reflection from the front face of the lip. A significantly lower angle (i.e., a flow turned to a lesser degree) near the wall was found for specular reflection from the front face of the lip for the knife-edge shape. The calculations for the knife-edge lip, then, show both a lowered flux and lowered flow angle in the backflow region when specular reflection is used for collisions of argon with the front face of the lip.

With respect to the apparent lack of effect of surface accommodation coefficient for the square-lip shape, it is interesting to look in a little more detail at the condition of the gas near the front of the lip. The number density profiles at the outer edge of the lip (profile A-A) for the square- and knife-edge lips with diffuse and specular reflection are shown in Figs. 11 and 12. For both the square and knife-edge lips, the number density and velocity (not shown) very close to the wall are lower for diffuse reflection and the temperature is higher. This is expected when there is full accommodation with the wall, which is hotter than the gas temperature in the region directly in front of the front face of the lip. When gas particles interact with the wall in diffuse reflection, they heat up, creating a temperature boundary layer. As a result, the number density and velocity are reduced from the case with no accommodation (specular reflection). This process occurs only very close to the wall (a few tenths of a millimeter) for the square lip, but extends out to about a millimeter for the knife-edge lip.

The lowering of the number density and velocity and the increase in temperature near the wall for diffuse reflection are also more pronounced for the knife-edge lip than for the square lip. The angle near the wall for the knife-edge lip was found to be lower for specular reflection, indicating that more of the flow will be directed into the forward flow region, reducing the total backflow (Fig. 11). The angle near the wall for the square lip was identical for both specular and diffuse reflection. This behavior combined with the smallness of the region affected by the wall conditions for diffuse reflection results in no appreciable change in the backflow flux for the square lip. For the knife-edge lip, the change in angle and the large extent of the region affected by the wall produces the large difference in backflow flux seen for this lip shape for diffuse and specular reflection.

Lip Surface Temperature

The effect of change in the temperature of the front surface of the lip on the backflow flux is shown in Table 2 for diffuse reflection. All of the results in this section are for a lip thickness of 0.8 mm. Despite the fact that the temperature near the front surface of the lip increases dramatically as the surface temperature increases, and despite the increase in the extent of the temperature boundary layer, the backflow flux for the square lip does not change significantly when the lip surface temperature is increased. The angle profile along B-B was also identical for the three temperature cases for the square lip.

For the knife-edge lip, the total backflow flux increases with lip surface temperature, to a degree that the total calculated flux into the backflow for a lip temperature of 10,000 K is as high as the flux for the square lip shape at that temperature. The number density and velocity profiles into the backflow region (profile B-B) for the knife-edge lip shape for the different lip temperatures are shown in Figs. 13 and 14. It is interesting that the number density profile is actually lower for the higher temperatures, but that the velocities increase substantially for the higher temperatures, which accounts for the increase in flux. The angle profile also increases somewhat with increasing lip temperature (Fig. 14). The number density and temperature profiles at a position along the outer edge of the lip (A-A) are shown in Figs. 15 and 16. The drop in number density with increasing lip temperature is noted again at this spatial position. There is a substantial rise in the gas temperature near the lip for increasing lip temperature, this increase in gas temperature being much larger than for the square lip shape. The velocity also shows a significant increase with lip surface temperature in this region.

The interaction of the gas with the front surface of the lip is again seen to be much more important for the knife-edge-shaped lip than for the square shape, similar to the results seen previously in the diffuse and specular reflection analysis. The increase in gas temperature near the lip increases the number of collisions in the region, allowing the gas to obtain a higher velocity that, despite the decrease in number density, increases the total flux into the backflow for the knife-edge lip. This effect is too small for the square lip shape to affect the backflow significantly.

Table 2 Relative backflow flux for different lip surface temperatures (0.8-mm lip)

	Lip temperature, K		
	300	1500	10,000
Square	1.0	0.966	1.186
Knife	0.485	0.527	1.378

Effects of Gas Starting Conditions

Number Density

To investigate the effects of the starting number density of the gas on the backflow structure, the number density at the start-line 0.15 mm upstream of the exit plane of the tube was increased by a factor of 10, and the calculations were repeated for various lip thicknesses for the knife-edge and square-edge lips. The boundary-layer profile was kept the same as before, with a multiplier used to change the numeric value of the number density, keeping all of the other gas flow parameters the same. A full-region run was conducted in each case to get a new start-line at the bottom of the lip, and a lip-region/backflow calculation was then run. The total flux into the backflow for the baseline case and for a number density a factor of 10 higher than the baseline case ($10 \times$ ND) is compared in Figs. 2 and 3. The calculated number density of the flow for the higher-number-density cases has been normalized by the number density multiplication factor (10).

It is apparent that the backflow flux does not scale directly with the starting number density. Specifically, the normalized

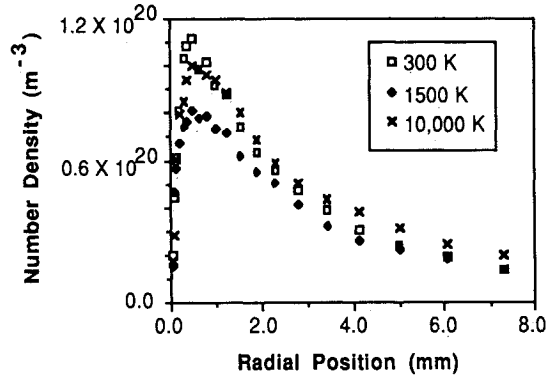

Fig. 13 Number density profile along B-B for 0.8-mm-thick knife-edge lip. Variation with lip temperature.

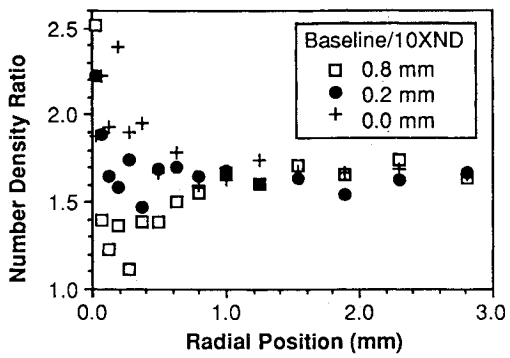

Fig. 14 Velocity profile along B-B for 0.8-mm-thick knife-edge lip. Variation with lip temperature.

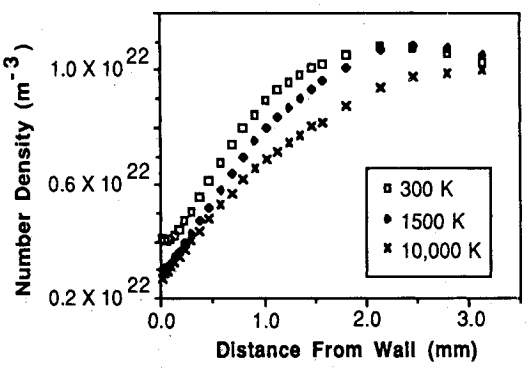

Fig. 15 Number density profile along A-A for 0.8-mm-thick knife-edge lip. Variation with lip temperature.

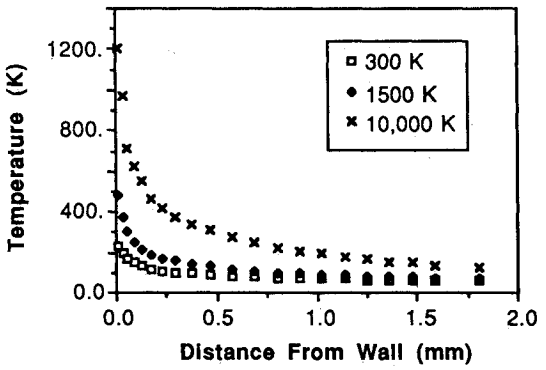

Fig. 16 Temperature profile along A-A for 0.8-mm-thick knife-edge lip. Variation with lip temperature.

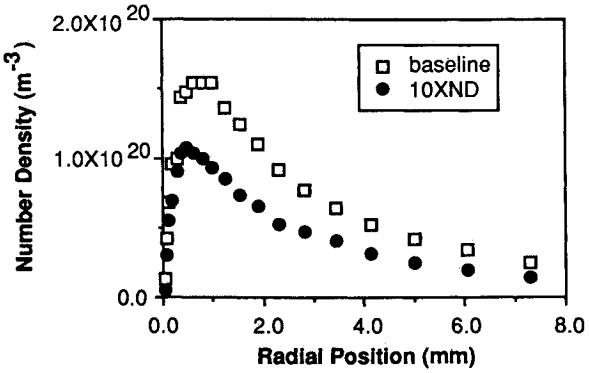

Fig. 17 Number density profile along B-B for 0.8-mm-thick square-edge lip. Comparison of baseline and 10 × ND starting conditions. Number density is normalized by starting number density multiplier.

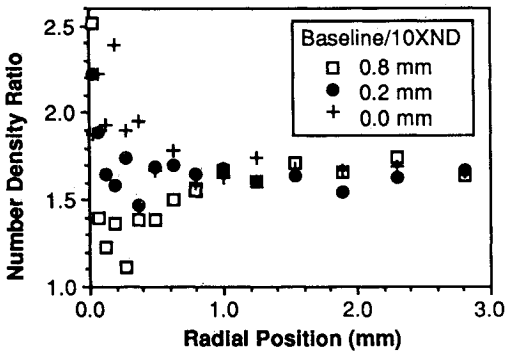

Fig. 18 Number density ratio profile along B-B for 0.8-mm-thick square-edge lip. Ratio between baseline and 10 × ND conditions. Number density is normalized by starting number density multiplier.

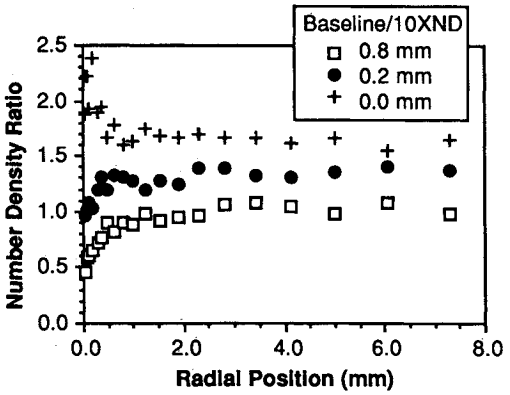

Fig. 19 Number density ratio profile along B-B for 0.8-mm-thick knife-edge lip. Ratio between baseline and 10 × ND conditions. Number density is normalized by starting number density multiplier.

flux drops about 40% for the higher-number density for the 0.0-mm lip thickness. For the square-shaped lip, the normalized flux for the higher-number density case approaches the values for the lower-number density as the lip thickness increases. For the knife-edge lip, the normalized flux for the higher-number density is very close to that for the lower-density case for a lip thickness of 0.2 mm, and then is higher than that for the lower-density case for larger-lip thicknesses (Fig. 2). Additionally, the difference in the normalized flux for the knife-edge lip compared to the square-edge lip is smaller for the higher-number density case than for the lower-number density case (Fig. 3).

There will be an increase in the total number of collisions when there are more gas particles in the flow, and this change in the collisional process can alter the velocity and angle profiles into the backflow region and, in addition, can change the position in the flow where the breakdown of translational equilibrium occurs.[13] A delay in the decoupling of the parallel translational mode from the perpendicular mode would be expected to increase the directed velocity of the flow, since this delay would allow more energy to be available for the expansion of the gas before energy is frozen into the parallel mode and is no longer available for conversion to directed motion of the gas. Bird's breakdown parameter[7] exceeds the value of 0.05 (usually assumed to define the onset of translation nonequilibrium) inside the tube just upstream of the exit plane for the lower-number density case, but not until well into the external expansion flow for the higher-number density case. In both the square- and knife-edge cases, the velocities were found to be higher into the backflow region for the higher-number density case for all lip thicknesses. Additionally, the velocities for the 10 × ND cases were found to be proportionately higher than the corresponding baseline velocities as the lip thickness increases, with the knife-edge lip showing a stronger propensity for this trend.[14]

The normalized number density profiles into the backflow region (along B-B) show a more complex behavior than the velocity profiles, as shown in Figs. 17–19. For the square-edge lip, the normalized number densities are always higher for the baseline case (Fig. 17), and the ratio between the normalized number densities for the baseline and 10 × ND cases increases with decreasing lip thickness (Fig. 18). Consequently, the decreased velocities (with increasing starting number density) are not enough to change the trend set by the number density profile, which is to reduce the normalized flux with increased starting number density. For the knife-edge lip, the normalized number densities for the baseline case are higher than those for the 10 × ND case for the thin lips, but are lower for the thicker lips (Fig. 19). As a result, the normalized flux for the knife-edge lip is smaller for the higher starting number density case for thin lips, is about the same as the baseline condition for a lip thickness of 0.2 mm, and then is higher than the baseline condition for the larger lip thickness (Fig. 2). For the knife-edge lip, the normalized flux for the higher starting number density levels out at a value 50% higher than the flux for the baseline condition for the thickest lips used in this analysis. This is in contrast to the square-lip results, where the normalized flux for the 10 × ND cases are all less than the baseline case, and where the difference in normalized flux between the baseline and 10 × ND cases decreases with increasing lip thickness (Fig. 2).

For both high starting number density cases (square and knife edge), the increase in velocity is a direct indication that the translational mode is in equilibrium longer than for the lower starting number density cases. The pattern of change in the normalized number density is another, more complicated, matter. The angle profiles in the backflow region are similar for the two lip shapes (slightly higher angle for higher number density), therefore the flow angle in this region does not yield any information about the difference in number density behavior. The horizontal profiles of flow angle in the top row of cells in front of the lip (A-A in Fig. 1) do not change with number density for the square lip, and change only a few degrees (and only in a region near the 1-mm position) for the knife-edge lip; and so once again the angle profile does not give a significant clue about the backflow behavior. For the higher starting number density case, the temperature profiles in front of the lip (A-A) show a slightly increased temperature near the face of the lip for the 0.8-mm knife edge and a similar but weaker trend for the 0.8-mm square lip. For the 0.2-mm lip, the temperature was lower for the square-edge and approximately the same for the knife-edge lip near the lip face. The gas is accommodating more to the surface for thicker lips and more for the knife edge than for the square edge. The number density profile in the lip region for the knife-edge lip shows a significantly *lower* normalized number density within 0.6 mm of the wall for the higher starting number density,

whereas the normalized number density is only slightly lower in that region for the square lip (for all lip thicknesses). The velocity profiles are essentially the same in the lip region for the knife-edge lip, and for the square-edge lip the velocities are slightly higher for the higher number density case.

The correlation of the flow parameters in the region in front of the lip to the backflow number density is not clear. Certainly the lower normalized number density in front of the lip for the 0.8-mm knife-edge lip for the high starting number density is somewhat curious, since the number density is higher in the backflow for this case. The molecules are "piling up" in front of the lip more for the lower starting number density case. This may be related to the degree of nonequilibrium in the translational mode and to the difference in accommodation to the surface. The relationship between the number density profile in front of the lip and the number density profile in the backflow is similar to that found when comparing the square-edge to knife-edge lip results, i.e., the number density is lower for the square-edge lip in front of the lip, but larger in the backflow region. In that case, the difference was explained by the larger angle in front of the lip for the square edge. For the high vs low starting number density comparison, the angles do not change significantly, and so this argument does not apply.

The interaction of the (translationally nonequilibrium) flow with the wall results in the behavior of the number density being different for the different lip shapes. This interaction between the characteristics of the gas expansion and the collisions of the gas with the wall is obviously a complex one not easily predicted without detailed modeling of the type employed here.

Temperature

An investigation of the effects of starting gas temperature was conducted using a similar technique as was used for investigation of starting number density effects in the previous section. The calculation was started at the position 0.15 mm upstream of the tube exit plane, with the starting gas temperature multiplied by factors of 5 and 10 in two separate calculations. The total flux into the backflow region for both lip geometries is compared in Table 3. An increase in the starting gas temperature produces a significant increase in the total backflow flux for both lip geometries. A large increase in the flow velocity with increasing starting temperature combines with a smaller but still significant increase in backflow number density near the wall to produce the resulting large difference in total backflow flux. There was only a small increase in flow angle into the backflow region between the standard case and the 5 × T case, and no change in flow angle into the backflow with increases of temperature above the 5 × T case.

An increase in the starting gas temperature increases the number of collisions in the flow which allows the flow to stay in equilibrium longer and consequently produces a higher flow velocity, as was the case when the starting number density was increased. The number density in the backflow increases with increasing starting temperature, which is somewhat contrary to the expected decrease due to the change in the expansion properties as seen when the starting number density was increased. If we look at the horizontal profile of the number density at the outer edge of the square lip (A-A) before the flow turns and enters the backflow region (Fig. 20), we see that the number density does drop with increasing starting temperature for the area of the flow 1 mm out from the wall. Close into the lip surface (Fig. 21), the number density increases with increasing starting temperature. It is this part of the flow that turns and enters the backflow region. The reason for this increase in number density can be deduced from the profile of the temperature at the outer edge of the lip (Fig. 22). Comparison of the temperature normalized by the starting temperature multiplier shows that the normalized temperature drops with increasing starting temperature. The increase in temperature in this region with increasing starting temperature is not keeping up with the increasing starting temperature due to the interaction with the cooler wall surface. Consequently, the number density change with starting

Table 3 Normalized backflow flux for different starting gas temperatures (0.8-mm lip)

	Temperature Multiplier		
	1	5	10
Square	1.0	2.486	4.130
Knife	0.485	1.171	1.757

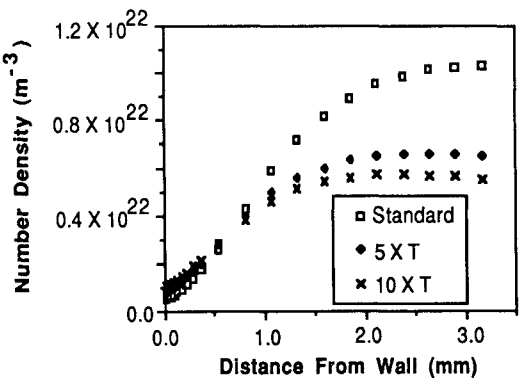

Fig. 20 Number density profile along A-A for 0.8-mm-thick square lip. Variation with starting gas temperature.

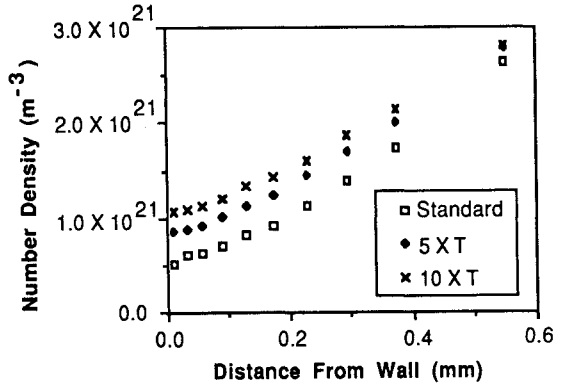

Fig. 21 Number density profile along A-A for 0.8-mm-thick square lip (expanded). Variation with starting gas temperature.

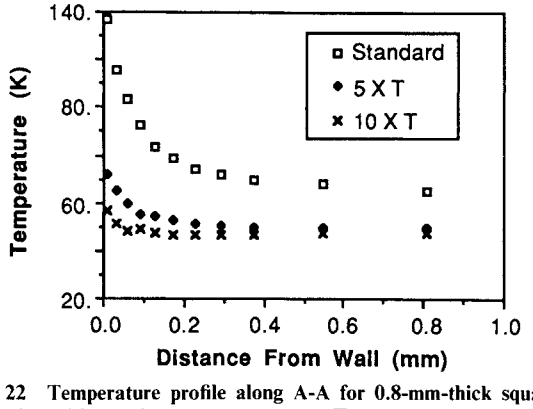

Fig. 22 Temperature profile along A-A for 0.8-mm-thick square lip. Variation with starting gas temperature. Temperatures are normalized by the corresponding starting temperature multiplier.

temperature reverses direction as one approaches the front lip surface (Figs. 20–21).

Summary and Conclusions

The structure of the flow of argon through a 4-mm-diam tube, around the tube lip, and into vacuum has been investigated using the Direct Simulation Monte Carlo technique. Two cases, a squared-off lip and a knife-edge lip, have been compared, and the results show that the shape and thickness of the lip have a significant influence on the flowfield. It can therefore be concluded that the collisional interaction of the gas with the front face of the lip makes a major contribution to the resulting characteristics of the flow into the backflow region.

The type of surface interaction and the temperature of the front surface of the lip used in the calculation do not affect the backflow for the square lip shape, but have a pronounced effect on the backflow for the knife-edge lip. The number density of the gas has a significant effect on the backflow due to changes in the collisional processes in the expansion flow, delaying the freezing out of the parallel component of the random motion of the gas, which consequently supplies more energy to the direct motion of the gas. The same type of process occurs when the overall temperature of the gas is increased, causing the total backflow flux to increase substantially with increasing gas temperature.

It must be emphasized that the results presented in this paper are for a single monatomic gas flowing to pure vacuum with no background gas interactions. In the actual cases of interest, there will always be some background gas moving at high velocity with respect to the emitted plume flow, which may be made up of a number of different molecular weight species. Consequently, any conclusions with respect to spacecraft contamination processes must wait for a more complete modeling effort including background gas interactions, which can be quite large,[15] as well as the effects of gaseous separation of the various species as they expand around the lip.[11,15] In addition, direct comparison to experimental data will also be necessary before these types of calculations can be reliably used to predict the structure of the backflow for actual rocket nozzles.

Acknowledgment

This work was performed under Air Force Astronautics Laboratory Contracts F04611-83-C-0046 and F04611-88-C-0020. Special thanks are due to Dr. Graeme Bird for his continued cooperation and guidance in the use of the Direct Simulation Monte Carlo code. Frank Frederick wrote the graphics code for the Apple Macintosh computer that was used to produce Figs. 4 and 5.

References

[1]Boynton, F. P., "Exhaust Plumes from Nozzles with Wall Boundary Layers," *Journal of Spacecraft and Rockets*, Vol. 5, Oct. 1968, pp. 1143–1147.

[2]Seubold, J. G., "Use of Viscous Nozzle Flow Program and the Method of Characteristics Plume Program to Predict Plume Expansion in the Back Flow Region for Small Thrusters," *Proceedings of the JANNAF 9th Plume Technology Meeting*, CPIA, Silver Spring, MD, Pub. 277, April 1976, pp. 1–14.

[3]Smith, S. D., "Improvements in Rocket Engine Nozzle and High-Altitude Plume Computations," AIAA Paper 83–1547, June 1983.

[4]Cooper, B. P., Jr., "Computational Scheme for Calculating the Plume Backflow Region," *Journal of Spacecraft and Rockets*, Vol. 16, July–Aug. 1979, pp. 284–286.

[5]Simons, G. A., "Effect of Nozzle Boundary Layers on Rocket Exhaust Plumes," *AIAA Journal*, Vol. 10, Nov. 1972, pp. 1534–1535.

[6]Greenwood, T., Seymour, D., Prozan, R., and Ratliff, A., "Analysis of Liquid Rocket Engine Exhaust Plumes," *Journal of Spacecraft and Rockets*, Vol. 8, Feb. 1971, pp. 123–128.

[7]Bird, G. A., "Breakdown of Continuum Flow in Freejets and Rocket Plumes," *Rarefied Gas Dynamics*, edited by Sam S. Fisher, AIAA, New York, 1981, pp. 681–694.

[8]Bird, G. A., *Molecular Gas Dynamics*, Clarenden Press, Oxford, 1976.

[9]Pipes, J. G., Bailey, A. B., Price, L. L., Lewis, J. W. L., Matz, R. J., and McGregor, W. K., "SRM Plume Simulation Flow Field of a Mach 7.0 Nitrogen Expansion into Vacuum," *Proceedings of the JANNAF 13th Plume Technology Meeting*, CPIA, Laurel, MD, Pub. 357, April 1982, pp. 95–106.

[10]Chirivella, J. E., "Mass Flux Measurements and Conditions in the Backflow Region of a Nozzle Plume," AIAA Paper 73–731, July 1973.

[11]Hueser, J. E., Melfi, L. T., Bird, G. A., and Brock, F. J., "Rocket Nozzle Lip Flow by Direct Simulation Monte Carlo Method," AIAA Paper 85-0995, June 1985.

[12]Cline, M. C., "VNAP2: A Computer Program for Computation of Two-Dimensional, Time-Dependent, Compressible, Turbulent Flow," Los Alamos National Lab., Rept. LA-8872, Aug. 1981.

[13]Bird, G. A., "Breakdown of Translational and Rotational Equilibrium in Gaseous Expansions," *AIAA Journal*, Vol. 8, Nov. 1970, pp. 1998–2003.

[14]Campbell, D. H., "Translational Non-Equilibrium Effects in Expansion Flows of Argon," *Proceedings of the 16th International Rarefied Gas Dynamics Symposium*, AIAA, Washington, DC, (to be published).

[15]Hueser, J. E., Melfi, L. T., Bird, G. A., and Brock, F. J., "Analysis of Large Solid Propellant Rocket Engine Exhaust Plumes Using the Direct Simulation Monte Carlo Method," AIAA Paper 84-0496, Jan. 1984.